Proceedings of the 10th World Congress on Electrical Engineering and Computer Systems and Sciences (EECSS'24)
Barcelona, Spain – August 19 - 21, 2024
Paper No. ICBES 104
DOI: 10.11159/icbes24.104

Melanoma Classification Combining Browning Index and Deep Neural Networks

Edmilson Queiroz dos Santos Filho [1], Evandro Ottoni Teatini Salles[1], Jacques Facon [2], Patrick Marques Ciarelli[1]
[1]Departamento de Engenharia Elétrica, Universidade Federal do Espírito Santo,
Vitória, Brasil
edmilson.q.santos@edu.ufes.br; evandro.salles@ufes.br; patrick.ciarelli@ufes.br
[2]Departamento de Computação e Eletrônica, Universidade Federal do Espírito Santo,
São Mateus, Brasil
jacques.facon@ufes.br

Abstract - Cutaneous melanoma, which originates from melanin producing cells (a substance that determines skin color), is the rarest and most dangerous type of skin cancer. Due to its high ability to spread to other areas of the body, early detection of cutaneous melanoma is the main action for reducing its mortality rates. By using computer-aided diagnosis that integrates some tools, such as image processing and deep learning, it is possible to develop efficient computational non- invasive approaches to cutaneous melanoma segmentation and recognition tasks. Unlike traditional approaches that directly process colorful original images, we propose to previously use a pre-processing step to highlight the skin melanoma from the rest of the skin before the segmentation process. The proposed solution consists of employing indicators of browning, called Browning Index (BI), used in some areas of the food industry. Three BIs (Aimonino, Lunadei2, and Fetuga) were applied separately and together in the images. The segmentation process was performed through two thresholding techniques (Otsu and Lloyd) and the morphological Watershed technique. The melanoma classification process, applied to previously segmented images, employed three CNN models: VGG19, ResNet50, and Xception. The results of the experiments show that previously highlighting the region of skin melanoma through the browning index aids in the classification process. The most promising results were obtained with the combination of the IDAT PWBHEPL, Lunadei2 Browning Index, Lloyd thresholding technique, and Xception CNN model, with an F1 score value of 97.05%.

Keywords**:** Cutaneous Melanoma, Deep Learning, Image Processing, Browning Index, Image Classification

1. Introduction

The skin is the largest organ of the human body, it corresponds to about 15% of body weight and contains great variations in its extension [1]. At the bottom of the skin are melanocytes, which produce melanin. With sun exposure, melanocytes produce pigments, resulting in epithelial darkening. Groups of melanocytes form a non-cancerous structure called a nevus [2]. People with many nevi have a higher risk of developing melanoma.

Cutaneous melanoma is one of the least frequent types of skin cancer, but it is the most deadly. Due to its high possibility of causing metastasis, melanoma is responsible for about 75% of deaths associated with skin cancer [3]. This type of lesion, after its infiltration in the lower layers of the skin and in its most advanced phase, has a great possibility of metastasis and the chance of a cure is practically non-existent. Therefore, the main chance of cure is the early diagnosis of the disease.

To diagnose skin cancer, the patient must undergo a biopsy, which is the only form of definitive diagnosis. In this procedure, the entire lesion, or at least part of it, is removed to be analyzed by a specialist under a microscope. The analysis is intended to look for cancer cells and must generally be performed by two or more pathologists [4]. An impediment to this diagnosis occurring early is the population's lack of access to the healthcare system [5]. Unfortunately, according to the World Health Organization [5], the incidence of both non-melanoma and melanoma skin cancers has been increasing over the past decades. Given that early-stage diagnosis can prevent countless deaths, in this paper, we propose a methodology to improve the detection of melanoma skin cancer based on the browning index (BI) combined with a convolutional neural network (CNN).

Therefore, the idea is to provide a skin cancer diagnosis model that can reduce cases of misdiagnosis and increase the chances of the patient receiving treatment on time [6].

BI can be defined as purity of brown color and is one of the most common indicators of browning in food products containing sugar [7]. The objective of this paper is to present and evaluate a methodology for diagnosing melanoma skin cancer in dermoscopic images using BI and CNN. This method is relevant and promising because the use of BIs can support CNNs in the classification process, increasing their performance. To the best of our knowledge, no previous study in the literature has explored the BI with CNN for skin cancer detection [8]. The methodology was evaluated on the public International Skin Imaging Collaboration (ISIC) 2016 [9] challenge

dataset of dermoscopic images (Figure 1). Three CNN architectures were evaluated in this paper: VGG19 [10], ResNet50 [11], and Xception [12]. In our experiments, BI + CNN provided F1 score of up to 89.70%.

This paper is organized as follows. Section 2 describes CNNs and BIs. Section 3 gives an overview of the proposed methodology. Section 4 shows the experimental evaluations and discussions about them. Finally, Section 5 presents our conclusions and points out some future paths.

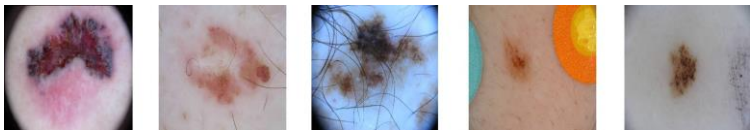

Fig. 1: Sample of skin lesions [9].

2. Methods

2.1. Segmentation

Image segmentation is the process of partitioning a digital image into image segments, according to the concepts of digital image processing and computer vision, which can be classified as regions of interest or backgrounds. Segmentation aims to simplify, change the representation, and highlight regions of an image so that something can make sense to the analyst. More precisely, image segmentation is the process of assigning an identifier to each pixel in an image so that elements with similar characteristics can be grouped [13].

Instead of directly using RGB original images as in traditional approaches, our proposal consists of previously enhancing the melanoma region before the segmentation process. Experiments carried out in [14] pointed out promising results in pre-processing the original images by BI, traditionally used in some areas of the industry. Concerning the challenge of detecting and recognizing skin melanoma lesions, Barbosa and Facon [14] justified this choice by the fact that the lesion usually has brown colors. Therefore, the hypothesis is that the use of the BI can be beneficial in highlighting melanoma lesions and their features, which can improve the detection and recognition of skin melanoma. Barbosa and Facon [14] show the application of three BIs (Aimonino, Lunadei2, and Fetuga) brought more quality in the segmentation of cutaneous melanoma. Their formulations are shown in Table 1: $BI_{Aimonino}$ [15], $BI_{Lunadei\ 2}$ [7], and BI_{Fetuga} [16]. In $BI_{Aimonino}$, k is a constant that represents the gain applied to the red channel. In this article, $BI_{Aimonino}$ was used with a value of k = 2.

Table 1: Three types of browning indexes [14].

Browning Index	Equation
Aimonino in RGB	$BI_{Aimonino} = kR - G - B$
Lunadei 2 in RGB	$BI_{Lunadei} = R - B$
Fetuga in L*a*b*	$BI_{Fetuga} = 100 - L$

Three binarization techniques were applied in this work: two based on threshold, Otsu [17] and Lloyd [18], and the Watershed [19] morphological technique. This resulted in seventeen combinations of methods with and without BI and threshold methods.

Figure 2 shows some images of melanoma and the enhancement that BIs can perform on lesions. BI are calculated according to the Table 1 using the RGB image. Then the obtained image is binarized using two thresholding techniques (Otsu or Lloyd) and the Watershed morphological process, thus generating a mask that is superimposed on the original image, in this way, the segmented image is obtained [8].

2.2. Deep Neural Networks

Deep learning is based on algorithms that model high-level abstractions, with meaningful concepts, from low-level ab- stractions, using multiple processing layers that perform linear and non-linear transformations [20]. Several deep learning architectures, such as CNN, have been applied in computer vision, producing state-of-the-art results [21]. CNN extracts fea- tures by filtering the images using convolutions and non-linear functions. The network learns which features are important to perform the assigned task [22].

There are three main types of layers in a CNN architecture: Convolutional layer, pooling layer, and fully connected layer [2].

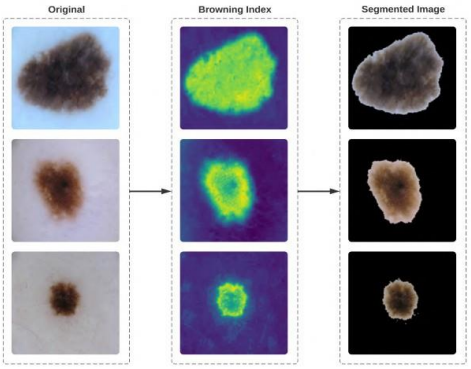

Fig. 2: Lesion enhancement by browning index and segmentation result.

Convolutional layers can be understood as sets of trained filters, represented in the form of activation matrices. Each filter learns a different structure of the image and is used as a feature extractor, generating maps representing that feature [23]. These layers may or may not be followed by a pooling layer, whose purpose is to statistically represent the previous layer. This layer uses the maximum or average function of a set of pixels within a predefined block that slides over the maps, so that the amount of data can be significantly reduced without significant loss [24].

Finally, the last layers of a CNN architecture are usually the fully connected layers, which are used to classify features extracted by the previous layers. A cost function is applied at the end of a CNN architecture, which aims to represent the error between the expected value and the prediction given by the neural network. This error is used in the backpropagation process to adjust the neural network weights (in the filters and fully connected layers) [25].

Other two relevant layers are the flatten layer and the dropout layer. Flatten layer is employed to transform a multidimensional input into a unidimensional output, an action necessary for the data to be applied in the fully connected layers. After the flatten layer, dropout was used in the evaluated architectures, which addresses the prevention of overfitting and provides a way to roughly exponentially combine many different neural network architectures efficiently [26].

In this paper, we used three CNN architectures: VGG19, ResNet50, and Xception. VGG is a neural network created by Karen Simonyan and Andrew Zisserman and it was developed for the ImageNet Large Scale Visual Recognition Challenge in 2014 [10]. It is currently one of the most used for image recognition and classification problems because of its simplified structure when compared to other convolutional networks. An accuracy of 98.37% was obtained in the classification of skin lesions into benign and malignant using Skin-Net [27] and an accuracy of 80.67% using VGG19.

The ResNet model (short for Residual Network) was proposed by engineers at Microsoft [11]. The structure can vary according to the number of layers, where the simplest has 18 and the most complex has 152 layers. This architecture has as its main characteristic the use of shortcut connections between convolution layers. The shortcut connections skip one or more layers and are arranged in the form of blocks, called residual blocks [28]. The technique used in [4] with the ResNet50 network produced 83% of accuracy with an F1 measure of 84%.

Xception is a convolutional neural network architecture based entirely on depth-separable convolution layers, which can be fully decoupled. Described as being a stronger version than the Inception architecture, it is thus called Xception, which stands for Extreme Inception [12]. The technique used in [29] with the Xception network produced an Area Under the Curve (AUC) value of 75% on the ISIC 2020 dataset.

ResNet50, VGG19, and Xception networks, as demonstrated by the literature analysis, are very effective methods in the task of classifying skin lesions. This indicates that the approach used in this article follows a robust concept for validating the accuracy of BI in supporting detection. Figure 3 shows a generic flow for a CNN.

2.3. Transfer Learning

Training a convolutional neural network is an extremely complicated and time-consuming task as it requires a large dataset with thousands of samples. Therefore, in some domains, especially in images, it is common to use models that were previously trained for some task (source) and reuse them for a similar task (target) [30].

Transfer learning is a procedure that can be used as a regularization method and is commonly used in deep learning approaches through the use of pre-trained models, which have been trained on a large set of benchmark

data to solve a problem similar to what we want to solve [31]. This procedure is useful to avoid overfitting problems if we have a small dataset for training when compared to the number of model parameters.

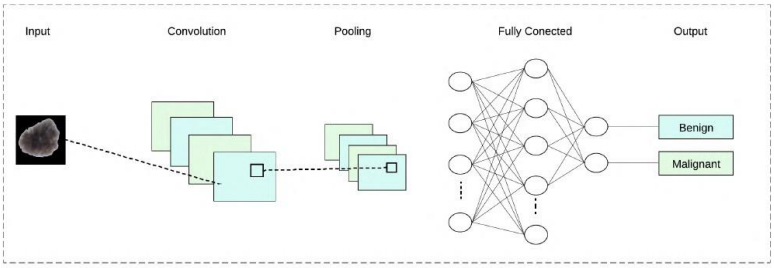

Fig. 3: CNN general architecture.

The networks used in this paper were previously trained with the ImageNet dataset, which is one of the most used datasets for the training of deep learning models [20].

Another procedure used in this article is fine-tuning, which is used to adjust the representations of higher-order features in the base model to make them more relevant to the specific task [32].

3. Methodology

In this section, we describe the methodology applied in this work, including the image processing technique to enhance regions of skin lesions, known as browning index (BI). Figure 4 shows a sequence of steps from input to classification. A brief description of each step employed is presented.

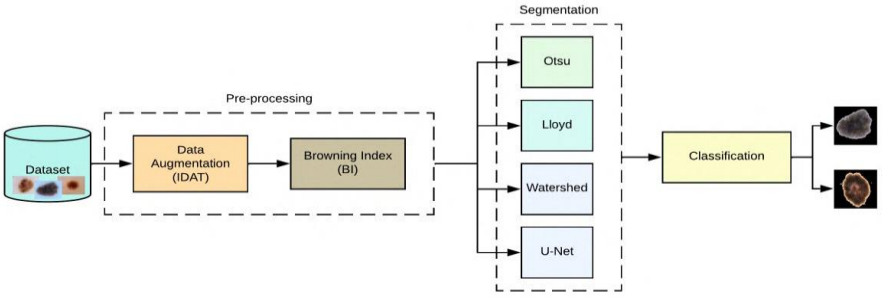

Fig. 4: Flowchart of the system.

The method proposed in this research aims to find a technique that supports CNN in its task of helping to diagnose cutaneous melanoma. Following the flowchart shown in Figure 4, BIs were initially calculated from the images and then segmented using thresholding techniques. Figure 2 visually shows the result of applying BI on images and, then, the segmen- tation of the images. Initially, the original images are in the RGB color model. Then the Aimonino, Fetuga and Lunadei BIs are calculated for each image. Therefore, the Otsu and Lloyd binarization methods and the Watershed morphological method are applied to obtain binary masks for skin lesions. Finally, pre-processing is completed by applying the mask to the original images. Furthermore, the images obtained from the BIs were also used directly in the CNNs. Thus, the images obtained serve as input for CNNs that classify lesions into two classes: melanoma or non-melanoma.

3.1. Dataset

The International Skin Imaging Collaboration (ISIC) is an academic and industrial partnership designed to develop re- search to reduce melanoma mortality. The ISIC datasets have become one of the leading repositories for researchers in machine learning for medical image analysis, especially in the field of skin cancer detection and malignancy assessment. They contain tens of thousands of dermoscopic images along with gold standard lesion diagnostic metadata [29].

The associated annual challenges have resulted in major contributions to the field, with works reporting measures far superior to human experts [9]. The overall focus of the challenge is to provide support to implement autonomous algorithms for the diagnosis of melanoma through dermoscopic images.

The ISIC 2016 challenge dataset consists of 900 training images and 379 test images. The training images are divided into 727 benign and 173 malignant images. Due to the relevant imbalance between the number of benign and malignant images, the following procedure was performed. First, all 173 malignant images were

selected. Then, 173 benign images were randomly selected. Finally, a data augmentation process was applied for the two subsets.

Instead of using the classic data augmentation techniques normally available to be used with deep networks, we used contrast and sharpness improvement techniques available in a tool developed for this purpose, called IDAT (Image Data Augmentation Tool) [33].

The methods used in [33] [34] were as follows:

- Histogram equalization by combining logarithm and power (PWBHEPL);
- Natural image enhancement by enhanced biogeography-based optimization with the migration operator (BBOBMO).

The BBOBMO and PWBHEPL techniques were applied to each of the benign and malignant images, generating two new images that replaced the original [34]. These techniques work by improving contrast/or sharpness, and the parameters are already automatically predefined by the IDAT tool. By using the IDAT, a new dataset composed of 346 malignant and 346 benign images was created.

3.2. Performance evaluation measure

To analyze the performance of the classifier, three statistical measures were considered: sensitivity, precision, and F1 score. The benign and malignant classes are evaluated and then the average between the two results is calculated. The definitions of these metrics are presented below.

Precision (Pre) means the ratio between correctly classified positive samples of a given class and all samples classified as positive, with false positives denoting the number of images incorrectly classified as positive samples.

Sensitivity (Se) is the ratio between the number of correctly classified positive samples of a given class and the total number of positive samples available for that class, including those that were incorrectly classified, where true positives and false negatives represent the number of samples correctly classified as positive and incorrectly classified as negative, respectively.

The F1 for a given class is calculated as the harmonic mean of the Se and Pre values for that specific class, resulting in a more global parameter to evaluate the performance of a classifier in each class.

More formally, these metrics can be defined as follows:

$$Pre = \frac{\text{true positives}}{\text{true positives} + \text{false positives}} \tag{1}$$

$$Se = \frac{\text{true positives}}{\text{true positives} + \text{false negatives}} \tag{2}$$

$$F_1 = 2 \text{ x } \frac{\text{Se x Pre}}{\text{Se} + \text{Pre}} \tag{3}$$

These metrics allow us to evaluate the performance of the classification algorithms considered in this work with reliability.

3.3. System Configuration

All experiments were run on a Windows 10 64 bits composed of an Intel(R) Core(TM) i7-11800H CPU @ 2.30GHz 2.30 GHz and 16 GB RAM. Furthermore, the deep extractors were implemented using the Python 3.9.12 programming language, Keras 2.1.4 a deep learning API with a Tensorflow 1.8 backend, and the classifiers were implemented using the Scikit-learn 0.19.1 library.

4. Experiments

Before carrying out the experiments, we balanced the dataset using the same number of images of benign and malignant classes, as the ISIC dataset is unbalanced. For this, the data augmentation technique was used, as described in Section 3.2. The images generated by the data augmentation process with the application of BIs were tested. For each class, the images were separated into 75% (260 images) for training, 15% (26 images) for validation, and 10% (17 images) for testing.

In training the U-Net network, the ISIC 2016 dataset from the segmentation task was used, consisting of 900 images and 900 ground truth binary masks, which were separated into 70% (630 images) for training, 15% (135 images) for validation and 15% (135 images) for testing. Initially, the indices $BI_{aimonino}$ with k = 2, $BI_{Lunadei2}$ and

BI_{Fetuga} were calculated according to Table 1. Then, the images were segmented using the Otsu, Lloyd and Watershed methods. The U-Net architecture used consists of a contracting path and an expanding path, which consists of the repeated application (five times) of two convolutions of 3 × 3, each followed by a rectified linear unit (ReLU) and a maximum pooling operation of 2 × 2 with step 2 for downsampling. The expansive path consists of an upsampling of the feature map followed by a 2 × 2 convolution that halves the number of feature channels, a concatenation with the correspondingly trimmed feature map of the contracting path and two 3 times3 convolutions, each followed by a ReLU. In the final layer, a 1×1 convolution is used to map each 64-component feature vector to the desired number of classes. U-Net training was carried out using the hyperparameters in Table 2. The binary cross-entropy function was chosen to minimize losses during training, as it is commonly used to quantify the difference between two probability distributions. The optimizer used was Adaptive Moment Estimation (Adam), which is an adaptive learning rate method. The early stopping technique was applied using the parameters that obtained the best result.

Table 2: U-Net hyperparameters.

Hyperparameters	Values
image size	256 × 256
learning rate	0.001
batch size	20
epoch	25
dropout probability	0.3
optimizer	Adam
loss method	binary crossentropy
early stopping patience	12

Table 3: The CNNs hyperparameters.

Hyperparameters	Values
initial learning rate	0.001
batch size	20
first decay steps (CDR)	500
alpha (CDR)	0.001
maximum number of epochs	200
patience (Early Stop)	100
performance monitor	val_loss

After, the images were segmented using the methods described in Section 2.1, and the images from each method were divided into training, validation, and test.

With this, the classification process began. The training data was shuffled to decrease the chance of overfitting during training. It is used batches size equal to 20 images. Then, two dense layers were added to each network with 128 and 64 neurons, with transfer function rectified linear units (ReLU), and another dense layer with 2 neurons and softmax activation function to predict the classes of the data. The Categorical Cross Entropy Function was chosen to minimize losses during training. The optimizer used was Stochastic Gradient Descent (SGD) with variable learning rate. The Early Stop technique was applied with a patience of 100 epochs for VGG19, ResNet50, and Xception. The function chosen to change the learning rate over the epochs was the Cosine Decay Restart function, whose learning rate value is reduced over the epochs and at a certain point is increased again. The values of the Cosine Decay Restart (CDR) hyperparameters are responsible for defining the learning rate that will be reduced to the minimum value, being calculated as the fraction of the initial learning rate multiplied by the alpha parameter. The hyperparameters for the VGG19, ResNet50, and Xception are presented in Table 3.

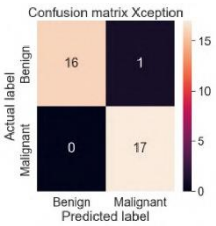

(a) Confusion Matrix of Lunadei with original images + Lloyd + Xception.

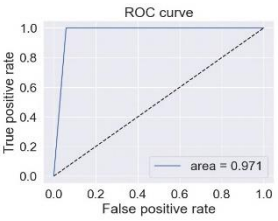

(b) ROC curve of Lunadei with original images + Lloyd + Xception

Fig. 5: The best result.

The figure 5 shows the best results obtained by the combination of techniques. The best result was obtained using IDAT method (PWBHEPL), BI Lunadei, Lloyd binarization and the Xception network, with an F1 score of 97.05%. This result can be seen from the values shown in the confusion matrix in Figure 5, which shows a low number of false positives and false negatives. The ROC curve is also shown in this figure.

Various results were obtained in this paper using combinations of IDAT methods (PWBHEPL and BBOBMO), BI methods (Aimonino, Fetuga and Lunadei), segmentation methods (Otsu, Lloyd, Watershed and Unet) and CNNs (VGG19, ResNet50 and Xception). Furthermore, the images generated by BI were also applied directly to the CNNs and, for example, the result obtained by the combination of Fetuga and Xception was an F1 score of 91.17%. To facilitate the reader's analysis, the best was selected, which are presented in Table 4. The results also show that the combination of Fetuga and Xception without segmentation is relevant, as it obtained a good result compared to segmented images. In Table 4 it can be seen that the most efficient BI in the task of highlighting the region of interest is Aimonino, which could be further studied in the future. Furthermore, CNN Xception stands out as the most efficient network in the classification task. The present approach obtained high results when compared to other research [35] [36] [37], which are presented in Table 4.

In the images presented in Figure 6, we can observe that there is low contrast between the background and the region of interest, a fact that makes the image analysis process difficult, and yet the proposed method proved to be robust both in segmentation and classification.

5. Conclusions

In this paper, we proposed the use of an innovative technique to highlight skin lesions, called browning index (BI). Three browning indices, BIaimonino, BILunadei2 , and BIFetuga, were combined with three CNN architectures, VGG19, ResNet50, and Xception, to classify cutaneous melanoma lesions. The best result was obtained by the combination of Lunadei, Lloyd and Xception, which returned an F1 of 97.05%. Another important point observed in the results is that the best BIs were Lunadei and Aimonino, which were present among the ten best results among the experiments carried out.

In future work, multitask network techniques will be applied, that is, the CNN will perform segmentation and classifcation tasks in the same architecture. BIs are also combined with approaches that extract information from the contours of skin lesions to increase the quality of skin lesion classification, since the skin cancer spot has irregular contours. It is also intended to propose a new specific BI for applications in skin lesions, thus being able to simplify the work of convolutional neural networks.

Table 4: Classification report.

Method	***Pre***	***Se***	F_1
PWBHEPL lunadei lloyd Xception	0.9722	0.9706	0.9705
PWBHEPL fetuga lloyd resnet50	0.9473	0.9412	0.9409
PWBHEPL aimonino_otsu Xception	0.9411	0.9411	0.9411
PWBHEPL fetuga lloyd Xception	0.9410	0.9410	0.9410
dermoExpert P1 [35]	0.9200	0.9200	0.9600
PWBHEPL fetuga Xception	0.9132	0.9117	0.9117
BBOBMO aimonino_otsu Xception	0.9131	0.9116	0.9116
BBOBMO lunadei Xception	0.9131	0.9116	0.9116
LCNet [36]	0.8188	0.8130	0.8105
Al-Masni [37]	0.8180	0.7140	0.8259

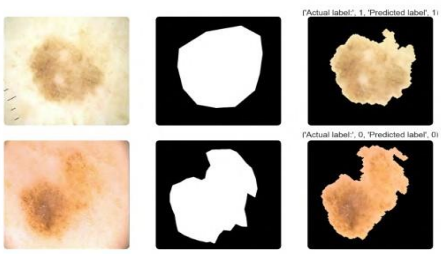

Fig. 6: Demonstration of the results obtained (Label 0 = Benign and Label 1 = Malignant).

Acknowledgements

The authors acknowledge the financial support given by CNPq (Conselho Nacional de Desenvolvimento Científico e Tecnológico) and FAPES (Fundação de Amparo à Pesquisa do Espírito Santo), numbers 598/2018 and 02/2019, respectively.

References

[1] F. Bernardo, K. Santos, and D. Silva, "Pele: Alterações anatômicas e fisiológicas do nascimento A` maturidade," *Revista Saúde em Foco*, vol. 11, 2019.

[2] L. B. Maia, A. Lima, R. M. P. Pereira, G. B. Junior, J. D. S. D. Almeida, and A. C. D. Paiva, "Evaluation of melanoma diagnosis using deep features," *International Conference on Systems, Signals, and Image Processing*, vol. 2018-June, 2018.

[3] Y. Li and L. Shen, "Skin lesion analysis towards melanoma detection using deep learning network," *Sensors (Switzerland)*, vol. 18, 2018.

[4] H. L. Gururaj, N. Manju, A. Nagarjun, V. N. M. Aradhya, and F. Flammini, "Deepskin: A deep learning approach for skin cancer classification," *IEEE Access*, vol. 11, pp. 50205–50214, 2023.

[5] WHO, "World health organisation - radiation: Ultraviolet (uv) radiation and skin cancer," *Who*, vol. 9, 2017.

[6] R. Zhang, "Melanoma detection using convolutional neural network," *2021 IEEE International Conference on Consumer Electron- ics and Computer Engineering, ICCECE 2021*, 2021.

[7] L. Lunadei, P. Galleguillos, B. Diezma, and L. Lie, "Evaluation of enzymatic browning in fresh-cut apple slices applying a multi- spectral vision system," in *International Conference on Agricultural Engineerig. AgEng*, pp. 1–11, 2010, 2010.

[8] E. Q. dos Santos Filho, E. O. T. Salles, J. Facon, and P. M. Ciarelli, "Browning index: An image processing technique to aid in the segmentation of skin lesions on dermatoscopic images," in *XVI Brazilian Conference on Computational Intelligence (CBIC 2023)*, 2023.

[9] D. Gutman, N. C. F. Codella, E. Celebi, B. Helba, M. Marchetti, N. Mishra, and A. Halpern, "Skin lesion analysis toward melanoma detection: A challenge at the international symposium on biomedical imaging (isbi) 2016, hosted by the international skin imaging collaboration (isic)," *arXiv e-print arXiv:1605.01397*, 2016.

[10] K. Simonyan and A. Zisserman, "Very deep convolutional networks for large-scale image recognition," *3rd International Confer- ence on Learning Representations, ICLR 2015 - Conference Track Proceedings*, 2015.

[11] K. He, X. Zhang, S. Ren, and J. Sun, "Deep residual learning for image recognition," *Proceedings of the IEEE Computer Society Conference on Computer Vision and Pattern Recognition*, vol. 2016-December, 2016.

[12] F. Chollet, "Xception: Deep learning with depthwise separable convolutions," 2017.

[13] R. C. Gonzalez and R. E. Woods, *Digital image processing*. Upper Saddle River, N.J.: Prentice Hall, 2008.

[14] S. R. Barbosa and J. Facon, "Aplicações em Segmentação de Padrões Marrons," in *Anais Eletrônicos da Jornada de IC da Ufes*,
pp. 1–15, 2020, 2020.

[15] D. R. Aimonino, P. Barge, P. G. Comba, A. Occelli, and C. Tortia, "Computer Vision for Laboratory Quality Control on Frozen Fruit," in *Chemical Engineering Transactions*, vol. 44, pp. 1–6, 2015, 2015.

[16] G. Fetuga, K. Tomlins, and F. Henshaw, "Effect of variety and processing method on functional properties of traditional

sweet potato flour (“elubo”) and sensory acceptability of cooked paste (“amala”),” in *Master thesis, Federal University Of Agriculture, Abeokuta, 2014*, 2014.

[17] N. Otsu, “Threshold selection method from gray-level histograms.,” *IEEE Trans Syst Man Cybern*, vol. SMC-9, 1979.

[18] F. Morii, “A supervised lloyd algorithm and segmentation of handwritten japanese characters,” in *9th European Signal Processing Conference (EUSIPCO 1998)*, pp. 1–4, 1998.

[19] Y. Wu and Q. Li, “The algorithm of watershed color image segmentation based on morphological gradient,” *Sensors*, vol. 22, no. 21, 2022.

[20] R. V. M. da No´brega, P. P. R. Filho, M. B. Rodrigues, S. P. da Silva, C. M. D. Júnior, and V. H. C. de Albuquerque, “Lung nodule malignancy classification in chest computed tomography images using transfer learning and convolutional neural networks,” *Neural Computing and Applications*, vol. 32, 2020.

[21] J. Ahmad, H. Farman, and Z. Jan, “Deep learning methods and applications,” *SpringerBriefs in Computer Science*, 2019.

[22] M. Dildar, S. Akram, M. Irfan, H. U. Khan, M. Ramzan, A. R. Mahmood, S. A. Alsaiari, A. H. M. Saeed, M. O. Alraddadi, and M. H. Mahnashi, “Skin cancer detection: A review using deep learning techniques,” *International Journal of Environmental Research and Public Health*, vol. 18, 2021.

[23] R. Yamashita, M. Nishio, R. K. G. Do, and K. Togashi, “Convolutional neural networks: an overview and application in radiology,”

[24] Insights into Imaging, vol. 9, 2018.

[25] J. Gu, Z. Wang, J. Kuen, L. Ma, A. Shahroudy, B. Shuai, T. Liu, X. Wang, G. Wang, J. Cai, and T. Chen, “Recent advances in convolutional neural networks,” Pattern Recognition, vol. 77, 2018.

[26] K. Safdar, S. Akbar, and A. Shoukat, “A majority voting based ensemble approach of deep learning classifiers for automated melanoma detection,” 4th International Conference on Innovative Computing, ICIC 2021, 2021.

[27] N. Srivastava, G. Hinton, A. Krizhevsky, I. Sutskever, and R. Salakhutdinov, “Dropout: A simple way to prevent neural networks from overfitting,” Journal of Machine Learning Research, vol. 15, 2014.

[28] Y. S. Alsahafi, M. A. Kassem, and K. M. Hosny, “Skin-net: a novel deep residual network for skin lesions classification using multilevel feature extraction and cross-channel correlation with detection of outlier,” *Journal of Big Data*, vol. 10, p. 105, Jun 2023.

[29] A. Shrestha and A. Mahmood, “Review of deep learning algorithms and architectures,” *IEEE Access*, vol. 7, 2019.

[30] B. Cassidy, C. Kendrick, A. Brodzicki, J. Jaworek-Korjakowska, and M. H. Yap, “Analysis of the isic image datasets: Usage, benchmarks and recommendations,” *Medical Image Analysis*, vol. 75, 2022.

[31] S. J. Pan, J. T. Kwok, and Q. Yang, “Transfer learning via dimensionality reduction,” *Proceedings of the National Conference on Artificial Intelligence*, vol. 2, 2008.

[32] W. Rawat and Z. Wang, “Deep convolutional neural networks for image classification: A comprehensive review,” *Neural Compu- tation*, vol. 29, 2017.

[33] A. Ramdan, A. Heryana, A. Arisal, R. B. S. Kusumo, and H. F. Pardede, “Transfer learning and fine-tuning for deep learning-based tea diseases detection on small datasets,” *Proceeding - 2020 International Conference on Radar, Antenna, Microwave, Electronics and Telecommunications, ICRAMET 2020*, 2020.

[34] G. M. Gaede and J. Facon, “Data Augmentation Novo em Redes Neurais Convolucionais,” in *Anais Eletrônicos da Jornada de IC da Ufes*, pp. 1–14, 2020, 2020.

[35] A. Toet and T. Wu, “Efficient contrast enhancement through log-power histogram modification,” *Journal of Electronic Imaging*, vol. 23, p. 063017, Nov. 2014.

[36] M. K. Hasan, M. T. E. Elahi, M. A. Alam, and M. T. Jawad, “Dermoexpert: Skin lesion classification using a hybrid convolutional neural network through segmentation, transfer learning, and augmentation,” *medRxiv*, 2021.

[37] R. Kaur, H. GholamHosseini, R. Sinha, and M. Linde´n, “Melanoma classification using a novel deep convolutional neural network with dermoscopic images,” *Sensors*, vol. 22, no. 3, 2022.

[38] M. A. Al-masni, D.-H. Kim, and T.-S. Kim, “Multiple skin lesions diagnostics via integrated deep convolutional networks for segmentation and classification,” *Computer Methods and Programs in Biomedicine*, vol. 190, p. 105351, 2020.